Original Article

Estimating Absorbed Dose to Breast Adipose Tissue from Mammograms

Al Maqsudur Rashid, Rabin Dhakal, Hanna Moussa
Department of Mechanical Engineering, Texas Tech University, Lubbock, TX, USA

Abstract

Purpose: Breast cancer usually originates in the glandular tissue of the breast. However, inflamed adipose tissue surrounding glandular tissue may expedite the local growth of cancerous cells. Exposing adipose tissue to radiation during mammography might cause inflammation in adipose tissue. This inflammation depends on the dose, and thus on the energy deposited from the X-ray mammography. Therefore, estimating the absorbed dose to adipose tissue during mammography is essential in breast cancer research. **Materials and Methods:** Absorbed dose to adipose tissue in the breast is determined using a new geometrical (semi-elliptical) model and Monte Carlo N-Particle transport code (MCNP6). X-ray mammogram images of patient breasts were taken as the basis of the new compressed breast geometry. The source probability density used in the MCNP6 code was generated from a published X-ray spectrum corresponding to tube voltage and air kerma. The relationship between various mammogram parameters such as peak tube voltage, compressed breast thickness, and adipose tissue weight fraction versus estimated absorbed dose is established for analysis. **Results:** Significant influences of adipose tissue weight fraction on absorbed dose were observed. **Conclusion:** Estimating the absorbed dose to breast adipose tissue during mammography and patients' degree of obesity are important factors in breast cancer research.

Keywords: Absorbed dose, adipose tissue, mammogram, Monte Carlo N-Particle, X-ray

Received on: 16-02-2021 **Review completed on:** 11-05-2021 **Accepted on:** 11-06-2021 **Published on:** 08-09-2021

Introduction

Frequent medical screenings in health care have resulted in increased exposure to ionizing radiation. Specifically, annual mammograms have come into wide use to detect breast cancer at an early stage. The two-dimensional digital mammogram procedure consists of taking X-ray images of each breast at two different projections. The female breast has three primary regions: Region (1) is the skin, region (2) is the subcutaneous adipose tissue just beneath the skin, and region (3) is the mixed adipose and glandular tissue [Figure 1]. The thickness of these three regions is dependent upon the woman's age, degree of obesity, and physical activity.[1,2] The average glandular dose is the average dose absorbed in the glandular tissue. Recommended AGD levels are promulgated by agencies like the International Commission on Radiological Protection and the Institute of Physical Sciences in Medicine.[3]

The breast tissue contains different types of cells including epithelial, glandular, and adipose or fat cells. Radiologists and physicians estimate the risk of radiation in the breast based on the amount of absorbed dose in the glandular tissue. However, the breast also contains adipose tissue that varies depending on the women's body mass index (BMI). Research shows that obese women (BMI for the obese woman is equal or more than 30) have more fat mass within the breast, increasing the chance of inflammation and oxidative stress as a result of irradiation.[3] There is evidence of the influential role of adipose tissue in inducing breast cancer.[4] People with higher BMI or who are suffering from obesity are more susceptible to higher radiation doses from exposure to radiation for either diagnostic or treatment purposes. Radiation, apart from targeting cancerous cells, also affects adjacent cells and damages noncancerous cells. Given the high content of adipose tissue within the breast, especially in obese women, it is critical to assess the

Access this article online

Quick Response Code:

Website: www.jmp.org.in

DOI: 10.4103/jmp.JMP_27_21

Address for correspondence: Dr. Hanna Moussa, Department of Mechanical Engineering, Texas Tech University, Lubbock, Tx 79409, USA.
E-mail: hanna.moussa@ttu.edu

How to cite this article: Rashid AM, Dhakal R, Moussa H. Estimating absorbed dose to breast adipose tissue from mammograms. J Med Phys 2021;46:171-80.

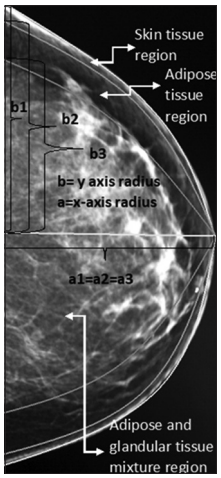

Figure 1: Actual mammogram X-ray image view of unknown patient' breast where the brighter show glandular and fibrous tissues while the darker areas show adipose tissue with a superficial layer of skin

effects of mammography X-ray exposure on adipocytes and how irradiated adipocytes alter other breast tissue cell types, possibly via secreted cytokines and hormones. Factors secreted by adipose tissue in response to radiation include inflammatory cytokines, levels of which are higher following ionizing radiation; the inflammatory cytokines then stimulate a cascade of events that damage surrounding tissues and organs.[5] Hence, irradiation causes inflammation, and adipose tissue is well established as an endocrine tissue that secretes hormones and other inflammatory molecules, irradiated adipocytes may increase breast cancer cell growth via this mechanism.

Very few studies have addressed the effects of low-dose X-ray radiation on the adipose tissue around microtumors found in the breast, especially among obese women.[6,7] A study has addressed the sensitivity of adipose tissue to radiation,[8] but it was conducted for acute exposure. The risk of low dose radiation has been studied in the breast, but no studies to date have addressed effects on adipose tissue surrounding breast cancer microtumors and only a few studies have focused on breast epithelial cells.[7] Thus, it is critical to understand the effects of low X-ray exposure on adipocytes since irradiation of adipose tissue may cause inflammation; this, in turn, may promote cancer cell growth in glandular tissue surrounded by breast adipose tissue.[9-11] Irradiation of these adipose tissues may indirectly affect other breast tissues through direct cell-to-cell communication or through factors secreted by adipocytes which affect normal glandular cells or cancerous cells and vice versa.[12-15]

Previous works estimated the absorbed dose to breast glandular tissue using the Monte Carlo technique, where a semi-circular cylindrical model is used to represent the compressed breast.[16] A voxelized breast model was also used with the Monte Carlo code for the same objective.[17] Moreover, software was developed by Bliznakova *et al*. in which the breast model consists of seven submodels, including the detailed tissue of the breast; this model was used to calculate the absorbed dose to the glandular tissue.[18] All these studies focused on estimating the absorbed dose to glandular tissue, not adipose tissue.

Although inflamed adipose tissue surrounding glandular tissue may expedite the growth of glandular cancer cells and estimating the absorbed dose to adipose tissue is essential in breast cancer research, little research has been done on estimating the absorbed dose to adipose tissue form X-ray mammogram. This study focuses on the estimation of the absorbed dose to breast adipose tissue using an accurate semi-elliptical model of the compressed breast as shown in Figure 1. This simple geometrical model is used in the MNCP6 code; the dimensions of this model were obtained from 61 X-ray images of different breast sizes.

Materials and Methods

Images of 31 patients' breasts with age group varied from 34 to 74 years was collected from Texas Tech University Medical Centre in Lubbock, Texas (Compact Disc that disabled patient identity), the included image viewing software were used to find the statistical detail of the breast dimensions [Table 1]. The dimensions of different regions of an 8-cm compressed breast in cranio-caudal[19] view are listed in Table 2 and shown in Figure 1. This software show what was the compressed thickness at the time when the mammogram images were taken. The actual X-ray images of 31 anonymous patients (31 images for the right breast and 30 images for the left one) were used to generate different compressed breast thicknesses [Table 3]. An average skin thickness of 0.15 cm,[18] and an average subcutaneous adipose tissue thickness (t_a) of 0.6 cm were obtained from the 31 patients' right breast images. In the MCNP6 geometry, the thickness of subcutaneous adipose varied from 0 cm in the major axis direction (a), to 0.6 cm in the minor axis (b) and the compressed thickness (z) directions. The brighter areas in the image [Figure 1] show glandular and fibrous tissues while the darker areas show adipose tissue with a superficial layer of skin.

It is assumed that this compressed thickness (under pressure) is a function of patient's breast size and degree of obesity. The 31-patient data [Table 1] shows that for large patients this thickness is higher, and it is also evident from the actual patient data. For large breast, compression paddle distance is also higher than medium or small breast. A range of the thickness from 4 to 8 cm is taken to represent small to large size. Furthermore, in the MCNP6 input, it is assumed that the subcutaneous fat (adipose tissue under the skin) thickness is constant for all breast thickness, and = 0.6 cm since its extremely difficult to correlate the fat thickness from one patient to another (R^2 value is only 0.29), also, the X-ray image data show no strong correlation between compressed thickness and adipose tissue under skin thickness. However, the percentage of adipose tissue in the mixed region (glandular and adipose tissue) is varied.

All digital copies of X-ray images were incorporated with built-in image analysis tools to measure dimensions and to pan,

Table 1: Statistical detail of dimension of 31 patient's right breast

Statistical features	Age (years)	Thickness (cm)	Width b (cm)	Breadth a (cm)
Mean	58.61	6.42	21.45	11.15
Median	61	6.80	20.90	10.50
SD	9.20	1.53	3.83	3.70
Maximum value	74	9.10	30	20
Minimum value	34	3.20	14.8	5.30

SD: Standard deviation

Table 2: Dimensional measurements of compressed breast image [Figure 1]

Mammogram data	Description	Dimension (cm)
a	Major axis radius	9.6
b	Minor axis radius	9.8
c	Skin layer	0.2
d	Adipose tissue under skin	0.8

zoom, or adjust image brightness. The major and minor axis radii, the average thickness of subcutaneous adipose tissue, and average skin thicknesses were calculated using the built-in dimensioning tool. Two fit equations were developed from those data to calculate the major and minor axis radii [*a1* and *b1* in Table 3] of the 1st half ellipse as a function of compressed breast thicknesses (Equations 1 and 2). These values were later incorporated into the geometry card of the MCNP6 code to accurately represent different compressed breasts.

$$a1 = -0.0234t^3 + 0.3508t^2 - 0.0943t + 3.667 \quad (1)$$

$$b1 = -0.0502t^3 + 0.9354t^2 - 4.6437t + 15.264 \quad (2)$$

where, t is the compressed breast thickness in cm. The 2nd half ellipse and the radii [*a2* and *b2* in Table 3] were calculated by subtracting the average skin thickness (0.15 cm) from *a1* and *b1,* respectively. For the 3rd half ellipse, the radii [*a3* and *b3* in Table 3] were calculated by subtracting the thickness of subcutaneous adipose tissue from *a2* and *b2*, respectively. These data in Table 3 were generated from best-fit data of an actual mammogram and utilized in the MCNP6 cell and surface cards to build standard compressed breast geometries.

Table 2 was for one single image (not used in MCNP6), whereas Table 3 was generated from the best-fit data of 31 anonymous patients (61 images of right and left breast). To simulate the X-ray image of the compressed breast in Figure 1, the MCNP6 geometry shown in Figure 2 was created. The whole model consists of three concentric semi-elliptical cylinders characterized by major and minor axes. The region between the first and second semi-elliptical cylinders represents a skin layer of 0.15 cm thickness. This skin thickness was considered based on the average breast skin thickness noted in the literature[20] and obtained from actual mammogram data.

The region between the second and third semielliptical cylinders represents subcutaneous adipose tissue, a 0.6 cm

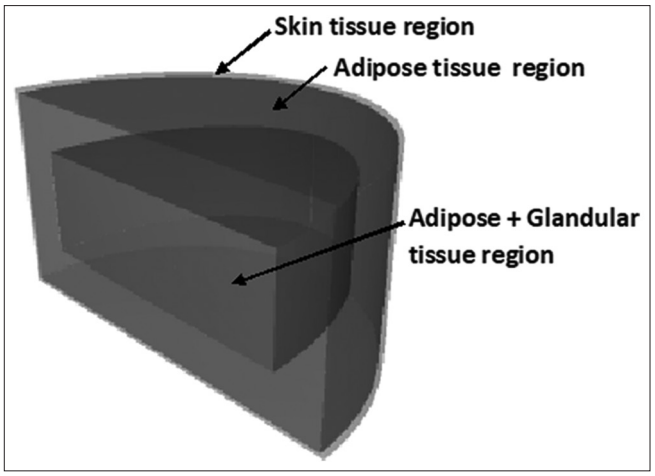

Figure 2: The MCNP6 geometrical model of compressed breast which consists of three concentric semi-elliptical cylinders

thickness is considered for all compressed thickness. The third, innermost semielliptical cylinder represents mixed adipose and glandular tissue. There is no correlation developed so far between the adipose tissue mass in the breast and the obesity degree, the percentage by mass of adipose tissue in the breast is chosen from 20% to 60%. Hence, the modeling considered the following percentages of mixed adipose and glandular tissue in the innermost semielliptical cylinder: (1) 20% adipose and 80% glandular; (2) 40% adipose and 60% glandular; (3) 50% adipose and 50% glandular and (4) 60% adipose and 40% glandular. The four types of materials defined in MCNP6 were: (a) skin, (b) adipose tissue, c) mixed adipose and glandular tissue, and d) air. The material elemental compositions for air and skin were taken from the material handbook recommended for radiation transport modeling[19] and the adipose and glandular tissue compositions from similar past studies of Hammerstein.[21] The volume fraction of the glandular tissue and adipose tissue in the mixed region can be calculated using the following equations:

$$v_a = 1 - \left(\frac{f_a \rho_g}{f_g \rho_a} + 1 \right)^{-1} \quad (3)$$

$$v_g = 1 - v_a \quad (4)$$

where ρ_a, ρ_g, v_a and v_g stand for the density of 100% adipose (0.93 g/cm^3) and 100% glandular tissues (1.04 g/cm^3) and their volume fractions, respectively.[22] And f_g and f_a represent mass fraction of glandular and adipose tissue. Furthermore, the mixture density can be obtained using the rule of mixture equation:

$$\rho_{mixture} = \rho_a v_a + \rho_g v_g \quad (5)$$

For example, for a mixture of 60% glandular and 40% adipose tissue, $f_g = 0.6$, and $f_a = 0.4$; from equations 3 and 4, $v_a = 0.43$ and $v_g = 0.57$; and from equation 5, the density of the mixture is 0.993 g/cm^3. Table 4 shows the elemental compositions of different breast tissues and Table 5 shows

Table 3: Different parameters of compressed breast geometry used for Monte Carlo N-Particle 6

CB thickness, t (cm)	1st half ellipse (outer)		2nd half ellipse (middle)		3rd half ellipse (middle)		Assumed skin thickness, t_s (cm)	Assumed adipose thickness under skin, t_a (cm)	Thickness of mixture region=(t-$2t_a$-$2t_s$) (cm)
	Major radius, a1 (cm)	Minor radius, b1 (cm)	Major radius, a2 (cm)	Minor radius, b2 (cm)	Major radius, a3 (cm)	Minor radius, b3 (cm)			
4	7.4	8.4	7.25	8.25	7.25	7.65	0.15	0.6	2.5
6	10.7	10.2	10.55	10.05	10.55	9.45	0.15	0.6	4.5
8	13.4	12.3	13.25	12.15	13.25	11.55	0.15	0.6	6.5
10	15.3	12.9	15.15	12.75	15.15	12.15	0.15	0.6	8.5

CB: Compressed breast

Table 4: Elemental composition (weight fraction) of different breast tissues

Elements	H	C	N	O	P	S	Cl	K	Ca
Adipose tissue	0.112	0.619	0.017	0.251	0.001	0	0	0	0
Glandular tissue	0.102	0.184	0.032	0.677	0.005	0	0	0	0
Skin	0.10059	0.2283	0.04642	0.619	0.0033	0.0016	0.0027	0.0009	0.00015

Table 5: Change in elemental weight fraction with different percentages of adipose and glandular tissue

Elements	H	C	N	O	*P*
20%-80% adipose + glandular	0.104	0.271	0.029	0.5918	0.0042
40%-60% adipose + glandular	0.106	0.358	0.026	0.5066	0.0034
50%-50% adipose + glandular	0.107	0.4015	0.0245	0.464	0.003
60%-40% adipose + glandular	0.108	0.445	0.023	0.4214	0.0026
80%-20% adipose + glandular	0.11	0.532	0.02	0.3362	0.0018

the calculated elemental compositions for different weight fractions of adipose and glandular tissue in the mixed adipose and glandular region.

The output of a mammography system is usually characterized as air kerma (mGy) per milliampere-seconds (mGy/mAs) at 100 cm from the focal spot. Air kerma is defined as the total kinetic energy of all charged particles released per unit mass of air,[23] and the focal spot is the point where the electron beam impinges on the tube anode. Table 6 tabulates the air kerma as a function of the tube voltage, the anode and filter type, and the half-value layer (HVL), where half value HVL is the thickness of a given material that reduces the photon intensity or air kerma rate of incident X-rays to one half of their initial value.[24]

The air kerma is then converted to air kerma at distances of 63.5, 61.5, 59.5, and 57.5 cm corresponding to compressed breast thicknesses of 4, 6, 8, and 10 cm, respectively, including the 2.5 cm air gap between the detector and bottom support plate. Figure 3 shows the pyramid-shaped air cell built around the compressed breast defined in the geometry card of MCNP6 code, a 0.3 cm thick rectangle of polycarbonate material on the top of the breast that represented the compression paddle plate of the mammogram unit.[25] The detector was not simulated in MCNP6, rather tally output in the three-separate compartment of the breast model is scored to calculate the average absorbed dose.

X-ray output data used in MCNP6

The mammogram X-ray image in Figure 1 was produced by a selenia dimensions full-field digital mammography (FFDM) system (Hologic, Inc.). In general, this system has a target anode made of tungsten (*W*), and optional rhodium (*Rh*) or silver (*Ag*) filters that are 0.052 mm thick for scanning.[26] The *Rh* filter is recommended for compressed breasts 1-5 cm in thickness, and the *Ag* for those 6-15 cm in thickness during manual exposure control. In automatic exposure control (AEC) mode, the machine decides on the optimal filter for best image quality and the lowest absorbed dose for the patient. The system's X-ray generator has a maximum tube current of 200 mA and an operating tube output voltage ranging from 20 to 49 kV.[25] In practice, the clinical range of energy varies from 25 to 39 kV. The system's maximum source to image distance (SID) is 70 cm, with an air gap of 2.5 cm between the bottom support plate and the detector, and the maximum field-of-view size of the X-ray detector is (29 × 24) cm. In MCNP6 simulation, the X-ray source is considered a point source with a spectrum of energy distributions. The *W* anode spectra similar to the Hologic Selenia Dimensions FFDM system were generated by using Tungsten Anode Spectral Model Interpolating Cubic Splines (TASMICS).[27]

The TASMICS is a Microsoft Excel spreadsheet, which is a free distributable Spreadsheet by Hernandez *et al*., capable of generating X-ray spectral data for the tube output voltage peak

Table 6: The tube output, air Kerma at 100 cm as a function of tube voltage, half value layer, and anode/filter combination

Tube voltage (kV)	Target (anode)	HVL (mm Al)	Filter	Air kerma (μGy/mAs) at 100 cm
25	W	0.48	Rh	11.4
28	W	0.52	Rh	16
31	W	0.56	Rh	20.4
31	W	0.63	Ag	27.4
34	W	0.66	Ag	33.8

HVL: Half-value layer

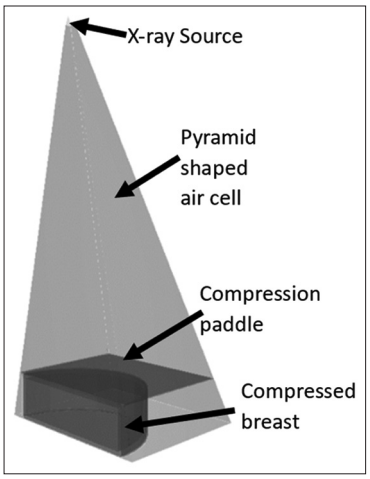

Figure 3: Pyramid-shaped air cell built around the compressed breast defined in the geometry card of MCNP6

kV between 20 and 640 kV, given the desired air kerma (mGy), filter, and HVL of the system.[26] The TASMICS is chosen because of its simplicity and also TASMICS demonstrated no statistically significant differences from Birch and Marshall and Poludniowski's spectral computational model over the wide range of tube potentials compared by Hernandez *et al*. Absorbed dose in the air (Air kerma) can be calculated using equation 6 where is the mass energy transfer coefficient of the material and is the energy fluence, which is energy passing through a unit cross-sectional area and can be derived by multiplying the photon fluence (ϕ) with photon energy (E).

$$K_{air} = \psi\left(\frac{\mu_{tr}}{\tilde{n}}\right)[J/kg] \quad (6)$$

Figure 4 shows example plots of X-ray spectra of 25–39 kV spectrums for both tungsten-silver (W/Ag) and tungsten-rhodium (W/Rh) anode-filter combinations. The horizontal axis of the spectra denotes the photon energy (keV) with 2 kV increments and the vertical axis denotes the fluence (number of photons per mm^2). Spectra similar to these were generated with TASMICS to calculate the output photon energy and its probability distribution [Table 7 for example] for MCNP dose calculations.

Verification of MCNP6 calculations

Air kerma verification

Air kerma values were calculated using the calibration chart [Table 6] for the Selenia Dimensions digital mammogram system;[24] this table lists the tube voltage, the HVL, the type of filter used, and the air kerma per mAs (in μGy/mAs) at 100 cm from the source (the X-ray focal spot). In turn, the calculated air kerma were used in the TASMIC program[27] to obtain the input parameters of the source card in MCNP6 (fluence probability vs. energy). To verify the MCNP6 result with the calibration data given in Table 6, the X-ray energy spectrum corresponding to air kerma of about 3.17 mGy, 28 kV, 86 mAs, and 0.52 mm Al HVL was considered as an input in the TASMIC program, where we adjusted the *Rh* filter to a thickness of 0.0586 mm, to obtain output spectra corresponding to an HVL of 0.52 (mm Al); This output spectra were used as a source card in the MCNP6 after normalizing each fluence to a source probability (fluence probability) corresponding to each energy. The estimated absorbed dose (D) in the thin air cell (20 cm × 24 cm × 0.1 cm) (air kerma) from MCNP6 using one million particles history was 1.663×10^{-6} MeV/particle passing all statistical checks; this value was converted to milli-Gray (mGy) by multiplying the total fluence per mm^2 [Table 7] by the entrance surface area (ESA) of the air cell (20 × 24) cm and dividing by the mass of air inside that air cell as follows:

$$D = \frac{(1.663\times10^{-6}\,\text{MeV}/p)\times(7.399*10^{11}P)}{\left(48cm^3\times1.293\times10^{-3}\frac{g}{cm^3}\right)\times\left(\frac{kg}{1000g}\right)} \times \frac{1Gy\times\left(1000\frac{mGy}{Gy}\right)}{\left(6.242\times10^{12}\frac{Mev}{kg}\right)} = 3.1766\,mGy \quad (7)$$

where 1 Gy is equal to 6.242×10^{12} MeV/kg. Comparing the estimated air kerma obtained from MCNP6 code (3.1768 mGy) to the air kerma used to generate the spectra in the TASMIC program, the percentage difference is <0.21%.

Absorbed dose verification

To verify the absorbed dose (D) to adipose tissue in the mixed region, the following parameters were used. A broad, parallel photon spectrum corresponding to 29 kV and a current of 100 mAs, incident on 6 cm compressed breast that consist of three layers: skin, subcutaneous adipose tissue, and mixed adipose and glandular (80% adipose and 20% glandular) tissue. Analytical and stimulated (MCNP6) calculations were performed. For this purpose, the absorbed dose to

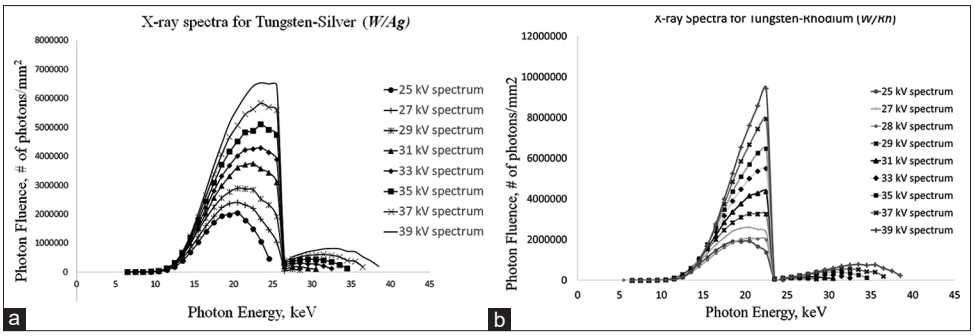

Figure 4: (a) The X-ray spectra of 25-39 kV spectrums for tungsten-silver (W/Ag); (b) The X-ray spectra of 25-39 kV spectrums for tungsten-rhodium (W/Rh)

Table 7: Tungsten anode spectral model interpolating cubic splines spectral data for 28 kV and 3.17 mGy air kerma, 0.52 half-value layer, and Rh filter

Photon energy (keV)	Fluence (photon/mm²)	Probability
5.5	9.83E-10	6.38E-17
6.5	7.13E-4	4.63E-11
7.5	1.55E00	1.01E-07
8.5	2.06E+2	1.33E-05
9.5	3.48E+3	2.26E-04
10.5	2.07E+4	1.34E-03
11.5	7.77E+4	5.04E-03
12.5	1.88E+5	1.22E-02
13.5	3.90E+5	2.53E-02
14.5	6.68E+5	4.34E-02
15.5	9.97E+5	6.57E-02
16.5	1.32E+6	8.53E-02
17.5	1.60E+6	1.03E-01
18.5	1.85E+6	1.20E-01
19.5	2.00E+6	1.30E-01
20.5	2.06E+6	1.30E-01
21.5	2.03E+6	1.30E-01
22.5	1.99E+6	1.30E-01
23.5	4.00E+4	2.59E-03
24.5	5.13E+4	3.33E-03
25.5	5.47E+4	3.55E-03
26.5	4.57E+4	2.97E-03
27.5	3.23E+4	2.09E-03
Total	1.54E+7	1.00E00

adipose tissue in the mixed region were calculated for each mono-energetic photon from the spectrum. The fluence to the mixed tissue region was considered as those photons that penetrated the skin and subcutaneous adipose tissue without interactions using Equation 8. The absorbed dose to adipose tissue in the mixed region was utilized using equation 9.

$$\varphi_m = \varphi_s \times \left(e^{-\left[\frac{\mu}{\rho}\right]_s \times \rho_s \times t_s} \right) \times \left(e^{-\left[\frac{\mu}{\rho}\right]_a \times \rho_a \times t_a} \right) \qquad (8)$$

$$D_a = \sum_i \left[\left\{ 1 - e^{-\left[\frac{\mu_{en(E_i)}}{\rho}\right]_m \times \rho_m \times t_m} \right\} \times E_i \times \varphi_m \times \frac{A_m}{mass_m} \times G_a \right] \qquad (9)$$

where subscript s, a, and m stand for skin, adipose, and mixture respectively, ϕ is the photon fluence, μ/ρ and μ_{en}/ρ were mass-attenuation and mass-energy absorption coefficients as a function of the elemental composition of each material and photon energy in the spectrum; the photon energy, mixture density, breast thickness, mass of the mixture and its area were expressed with symbols E_i, ρ, t_m, $mass_m$ and A_m, respectively. Finally, G factor (G_a) was utilized to separate the absorbed dose to adipose tissue in the mixed tissue only.

The estimated absorbed dose to 60% adipose tissue in the mixed tissue region from the above analytical solution was 0.351 mGy compared to the MCNP6 calculated absorbed dose of 0.482 mGy, which brought a relative error of 27%. This error was encountered due to simplifying assumptions of parallel broad beam radiation and neglecting the contribution of bremsstrahlung and the scattering and double scattering photons to the absorbed dose. Moreover, while photons that interacted with the skin and subcutaneous adipose tissue were removed from further calculation of the dose to the mixed tissue region in the analytical solution, the contributions of photons– which need to be considered-that interacted with the skin and subcutaneous adipose tissue to the absorbed dose in the mixed tissue region are included in the MCNP6 results.

Results

MCNP6 codes were utilized to calculate the absorbed dose to compressed breast thicknesses: 4 cm represents a small breast, 6 and 8 cm represents a medium breast, and 10 cm represents a large breast. In the MCNP6 simulations, energy deposition in adipose tissue was estimated as MeV per gram per particles (F6 tally output in MCNP6 code) and converted to the absorbed dose in the unit of mGy using equation 10.

$$D_a = \left[F_{6\,(MCNP6)}\left(\frac{MeV}{gm * p}\right) \times \varphi \frac{p}{mm^2} \times ESA\left(mm^2\right) \times \left(1.602 \times 10^{-7}\right) \frac{mGy}{\frac{MeV}{gm}} \times G_a \right] \quad (10)$$

where the total number of photons that interacted with the breast tissue (fluence multiplied by the ESA was computed by the procedure mentioned in the air kerma verification section. To separate the absorbed dose to adipose tissue alone from the total absorbed dose to the mixture region, a factor G_a expressed in equation 11[22] was utilized.

$$G_a = \frac{f_a\left(\frac{\mu_{en}}{\rho}\right)_a}{\left[f_a\left(\frac{\mu_{en}}{\rho}\right)_a + f_g\left(\frac{\mu_{en}}{\rho}\right)_g\right]} \quad (11)$$

where subscripts a and g stand for adipose and glandular tissue, respectively; μ_{en}/ρ represents the mass-energy absorption coefficient, and *f* represents weight fraction. These coefficients for adipose and glandular tissue were calculated [Table 8] using a parameterized polynomial equation given by Okunade[28] for the elemental composition and percentages by weight listed in Table 4 and the weighted average energy. Using the parameter in Table 9, G factor was calculated for 29 kV tube voltage and tabulated in Table 9.

Figure 5 illustrates the absorbed dose to adipose tissue using Equation 10 and the MCNP6 results, where all different thicknesses of breasts with 60% adipose weight fraction in the mixed tissue region were exposed to a fixed 100 mAs X-ray energy and 29 kV fluence with the tungsten anode and Rh filter. When exposed to the same X-ray generated from identical current and same tube voltage for 60% adipose tissue in the mixed tissue region, smaller breasts had a higher absorbed dose to adipose tissue compared to larger breasts. For the same X-ray current and tube voltage, the absorbed doses in adipose tissue gradually decreased as the compressed breast thickness increased from 4 cm to 10 cm (the compressed breast thickness is automatically determined by the mammogram machine for specific patient).

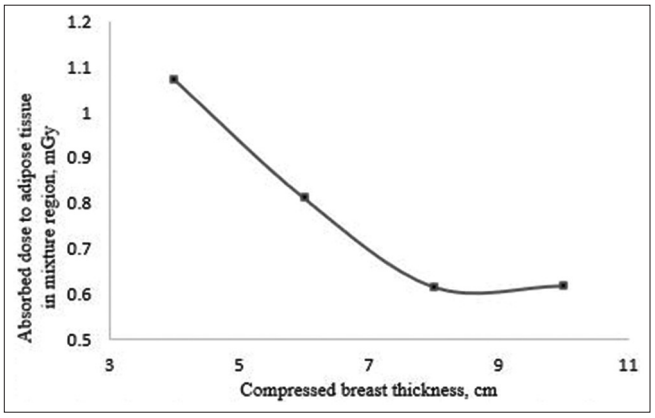

Figure 5: Absorbed dose to adipose tissue in the mixture region versus compressed breast thickness

Table 8: Mass energy absorption coefficients for adipose and glandular tissue

kV	Weighted average energy, E, keV	For glandular, $(\mu_{en}/\rho)_g$, cm²/g	For adipose, $(\mu_{en}/\rho)_a$, cm²/g
25	18.5	0.64	0.39
27	18.9	0.60	0.37
29	19.1	0.58	0.35
31	19.4	0.54	0.33
33	19.9	0.51	0.31
35	20.3	0.47	0.29
37	20.9	0.43	0.27
39	21.5	0.40	0.24

Table 9: G factor calculations for 29 kV tube voltage and different weight fractions in the mixture

f_g	$f_a=1-f_g$	ρ_g	ρ_a	v_a	$v_g=1-v_a$	Pmixture	$(\mu_{en})_g/\rho_g$, cm²/g	$(\mu_{en})_a/\rho_a$, cm²/g	G_g	G_a
0	1	1.04	0.93	1	0	0.93	0.58	0.35	0	1
0.1	0.9	1.04	0.93	0.91	0.09	0.94	0.58	0.35	0.15	0.85
0.2	0.8	1.04	0.93	0.82	0.18	0.95	0.58	0.35	0.29	0.71
0.3	0.7	1.04	0.93	0.72	0.28	0.96	0.58	0.35	0.41	0.59
0.4	0.6	1.04	0.93	0.63	0.37	0.97	0.58	0.35	0.52	0.48
0.5	0.5	1.04	0.93	0.53	0.47	0.98	0.58	0.35	0.62	0.38
0.6	0.4	1.04	0.93	0.43	0.57	0.99	0.58	0.35	0.71	0.29
0.7	0.3	1.04	0.93	0.32	0.68	1.0	0.58	0.35	0.79	0.21
0.8	0.2	1.04	0.93	0.22	0.78	1.02	0.58	0.35	0.87	0.13
0.9	0.1	1.04	0.93	0.11	0.89	1.03	0.58	0.35	0.94	0.06
1	0	1.04	0.93	0	1	1.04	0.58	0.35	1	0

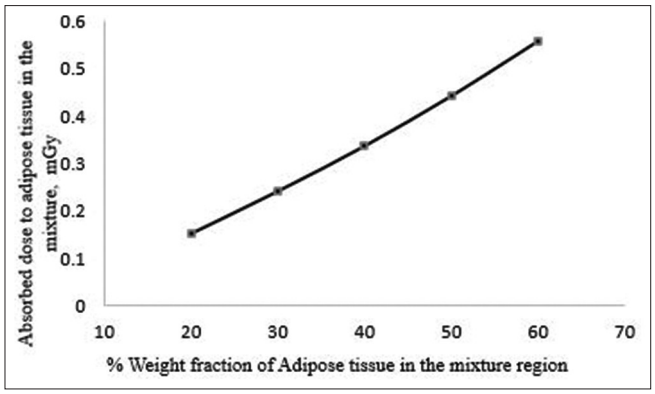

Figure 6: Absorbed dose to adipose tissue in the mixture region versus % weight fraction of adipose tissue

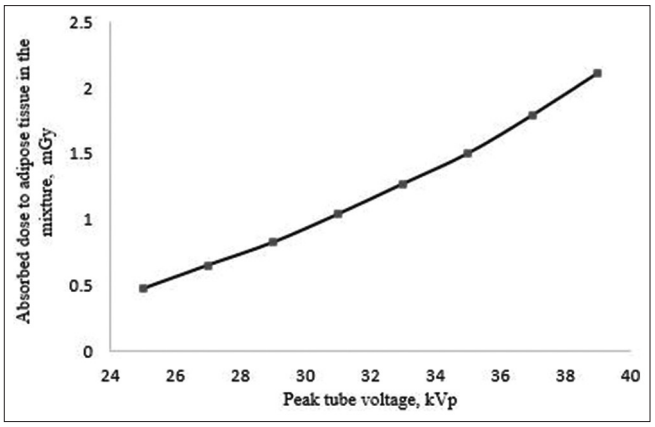

Figure 7: Absorbed dose to adipose tissue in the mixture region versus peak tube voltage

Tube output voltage kV and the current (mA) of the X-ray tube in the mammogram machine determine the energy and fluence of the output photons to be used;[25] At a fixed product of X-ray tube current and exposure time 100 mAs with peak voltage of 29 kV, the average absorbed dose to the adipose tissue in the mixed tissue region increases as the weight fraction of adipose tissue increases from 20% to 60% [Figure 6]. This is due to the accompanying increase in the elemental weight fraction of carbon and hydrogen atoms [Table 5].

Figure 7 shows the relation between peak tube voltage and corresponding absorbed dose to adipose tissue in the mixed tissue region for an 8 cm compressed breast with 60% adipose tissue at a constant 100 mAs using the *Rh* filter. The general trend of the absorbed dose shown in Figure 7 is to increase as peak tube voltage kV increases. A higher voltage in the X-ray tube will generate photons with higher kinetic energy and increases exposure since exposure is approximately proportional to the square of kV in the clinical energy range.[25] As a result, higher exposure due to increases in kV resulted in higher absorbed dose for the same mAs, filter, and compressed breast thickness [Figure 7].

The absorbed doses in Figure 8 were estimated using MCNP6 with input data generated using the AEC settings [Table 10] for the Hologic Selenia Dimensions FFDM system.[29]

In Table 10, as the compressed breast thickness increases, the machine automatically selects optimized settings for kV and mAs, and the correct filter to obtain the best image quality and minimize the X-ray dose to the patient. In automatic mode, the machine tends to choose higher kV and mAs as the thickness increases; for thicknesses greater than 7 cm, the *Ag* filter is usually selected.[26] When the AEC selected parameters [Table 10] were used in MCNP6, the absorbed dose to the adipose tissue in the mixed tissue region increased as the compressed breast thickness increased. As both kV and mAs increase, the photon energy and total photon fluence also increase, and consequently, the absorbed dose to the adipose tissue increases.

For 4 cm compressed breast thickness with 60% adipose weight fraction, the absorbed dose to adipose tissue in the mixed tissue region was 1.107 mGy [Figure 5] where the total absorbed dose for that region was 2.306 mGy. The G factor for 60% adipose tissue was calculated as 0.48 [Table 9] meaning that 48% of the total absorbed dose to the mixed tissue region was to the adipose tissue. Hence, women with breasts characterized as "fatty" have more risk of inflammation from mammogram X-ray exposure.

Table 10: Automatic exposure control settings for different compressed breasts in the Selenia Dimensions full-field digital mammography system

Thickness (cm)	kVp	mAs	Filter	HVL (mm Al)
4	28	71.3	Rh	0.52
6	31	150.3	Rh	0.55
8	32	164.3	Ag	0.64

HVL: Half-value layer

Discussion

The low absorbed dose may produce inflammation in adipose tissue. Given the amounts of adipose tissue within the glandular tissue of the breast, adipose tissue inflammation may also enhance cancer growth. Our study has parted away from conventional mammogram dosimetry study where the mean glandular dose is the primary metric of absorbed dose to the breast. Our primary goal was to estimate the absorbed dose in adipose tissue inside the third region (mixed adipose and glandular tissue) from various low energy X-ray during mammogram procedures, where in future research, we can correlate these absorbed doses in breast adipose tissue with inflammation, and subsequently with cancer and cancer risk. Using a dosimeter, we can easily measure the air kerma (entrance absorbed dose) for a given source; however, we cannot place the dosimeter inside the breast to measure the absorbed dose. Ultimately, using MCNP code to estimate the absorbed dose to adipose tissue inside the breast is a very practical and convenient way of simulating millions of particle interactions and consequently energy deposition.

Figure 8: Absorbed dose to adipose tissue in the mixture region (the input data were generated using automatic exposure control

Since it is difficult to estimate the skin thickness (first region) and the adipose tissue thickness (second region), we assumed an average thickness of 0.15 cm for the skin and 0.6 cm for the adipose tissue in the second region. Our elaborate study showed that with increased weight fraction of adipose tissue in the adipose-glandular region, absorbed dose also increased when we kept the breast compressed size, kV and mAs constant [Figure 6]. In other words, if two patients' breasts with the same age, exposed to the X-ray beam from mammogram machine with the same kV and mAs, the absorbed dose will be higher for the patient who has more adipose tissue in the breast.

Although AEC of the mammogram machine adjusts the X-ray kV and mA dynamically for each patient to optimize the dose received by patients and achieve best signal-to-noise ratio, it does not consider the percentage of adipose tissue in the breast. Thus, our approach, in considering fat mass is innovative and provides more accurate dosimetry estimates.

Conclusion

Research on adipose tissue inflammation is still in its rudimentary stage and has yet to be explored from a dosimetry perspective. In this work, we presented tabulated data of the absorbed dose to adipose tissue in the mixture region of compressed breasts during mammogram screening in the craniocaudal view for a commonly used mammogram system with MCNP6. These data will serve as a supplement to dosimetry characterizations and the role of adipose tissue irradiation on breast cancer initiation and tumor growth.

When current, exposure time and peak voltage were kept constant, the average absorbed dose in the adipose tissue of the mixed tissue region increases as the weight fraction of adipose tissue increases; therefore, women who are obese are the most vulnerable group to mammogram radiation exposure. Detailed dosimetry analysis will aid the researchers in this field in terms of exploring the cellular mechanism of low absorbed dose radiation to adipose tissue and its effects on adjacent cells.

In our work we theoretically estimated absorbed dose in adipose tissue for different tissue composition of adipose tissue and X-ray energy range Moreover, an empirical work can be performed in the form of animal studies to better understand whether these low absorbed doses can initiate inflammation and the degree of inflammation with *in vitro/in vivo* studies for mammogram risk assessment.

Acknowledgments

We would like to acknowledge and extend our gratitude to the University Medical Center Hospital Mammogram Department Supervisor, Mr. Philip Houghton, for providing us access to the mammogram database and technique charts of the mammogram machine.

Financial support and sponsorship

Nil.

Conflicts of interest

There are no conflicts of interest.

References

1. Schapira DV, Clark RA, Wolff PA, Jarrett AR, Kumar NB, Aziz NM. Visceral obesity and breast cancer risk. Cancer 1994;74:632-9.
2. Shuster A, Patlas M, Pinthus JH, Mourtzakis M. The clinical importance of visceral adiposity: A critical review of methods for visceral adipose tissue analysis. Br J Radiol 2012;85:1-10.
3. Valentin J. The 2007 recommendations of the international commission or radiological protection. Publication 1977;103:53-9.
4. Ligibel J. Obesity and breast cancer. Oncology (Williston Park) 2011;11:994-1000.
5. Siriwardhana N, Layman R, Karwandyar A, Patel S, Tage B. Inflammatory cytokines link obesity and breast cancer. J Metabolic Synd, 2012;1:2167-0943.
6. Soler D, Pampalona J, Tusell L, Genescà A. Radiation sensitivity increases with proliferation-associated telomere dysfunction in nontransformed human epithelial cells. Aging Cell 2009;8:414-25.
7. Hernández L, Terradas M, Martín M, Feijoo P, Soler D, Tusell L, *et al.* Increased mammogram-induced DNA damage in mammary epithelial cells aged *in vitro*. PloS One 2013;8:e63052.
8. Poglio S, Galvani S, Bour S, André M, Prunet-Marcassus B, Pénicaud L, *et al.* Adipose tissue sensitivity to radiation exposure. Am J Pathol 2009;174:44-53.
9. Little JB. Genomic instability and radiation. J Radiol Prot 2003;23:173-81.
10. Lu CW, Lo YH, Chen CH, Lin CY, Tsai CH, Chen PJ, *et al.* VLDL and LDL, but not HDL, promote breast cancer cell proliferation, metastasis and angiogenesis. Cancer Lett 2017;388:130-8.
11. Baek AE, Nelson ER. The contribution of cholesterol and its metabolites to the pathophysiology of breast cancer. Horm Cancer 2016;7:219-28.
12. Siriwardhana N, Kalupahana NS, Fletcher S, Xin W, Claycombe KJ, Quignard-Boulange A, *et al.* n-3 and n-6 polyunsaturated fatty acids differentially regulate adipose angiotensinogen and other inflammatory adipokines in part via NF-κB-dependent mechanisms. J Nutr Biochem 2012;23:1661-7.
13. Maqsudur Rashid A, Ramalingam L, Al-Jawadi A, Moustaid-Moussa N, Moussa H. Low dose radiation, inflammatio. Int J Radiat Biol 2019;95:506-15. [doi: 10.1080/09553002.2018.1484194].
14. Wu Q, Li B, Li Z, Li J, Sun S, Sun S. Cancer-associated adipocytes: Key players in breast cancer progression. J Hematol Oncol 2019;12:1-5.
15. Chu DT, Phuong TN, Tien NL, Tran DK, Nguyen TT, Thanh VV, *et al.* The effects of adipocytes on the regulation of breast cancer in the tumor microenvironment: An update. Cells 2019;8:857.
16. Verdú G, Leön A, Villaescusa J, Salas M, Cuevas M, Bueno F. Mammographic dosimetry using MCNP-4B. J Nucl Sci Technol 2000;37 Suppl 1:875-9.
17. Chen B, Shorey J, Saunders RS Jr., Richard S, Thompson J, *et al.*

An anthropomorphic breast model for breast imaging simulation and optimization. Acad Radiol 2011;18:536-46.
18. Bliznakova K, Bliznakov Z, Bravou V, Kolitsi Z, Pallikarakis N. A three-dimensional breast software phantom for mammography simulation. Phys Med Biol 2003;48:3699.
19. McConn RJ, Gesh CJ, Pagh RT, Rucker RA, Williams III R. Compendium of material composition data for radiation transport modeling (No. PNNL-15870 Rev. 1). Pacific Northwest National Lab. (PNNL), Richland, WA (United States) 2011.
20. Zastrow E, Davis SK, Lazebnik M, Kelcz F, Van Veen BD, Hagness SC. Development of anatomically realistic numerical breast phantoms with accurate dielectric properties for modeling microwave interactions with the human breast. IEEE Trans Biomed Eng 2008;55:2792-800.
21. Richard Hammerstein G, Miller DW, White DR, Ellen Masterson M, Woodard HQ, Laughlin JS. Absorbed radiation dose in mammography 1. Radiology 1979;130:485-91.
22. Boone JM. Glandular breast dose for monoenergetic and high-energy x-ray beams: Monte Carlo assessment 1. Radiology 1999;213:23-37.
23. Turner JE. Atoms, Radiation, and Radiation Protection. Hoboken, NJ : John Wiley and Sons; 2008.
24. Strudley C, Looney P, Young K. Technical evaluation of Hologic Selenia Dimensions digital breast tomosynthesis system. NHSBSP Equip Rep 2014;1307:1-33.
25. Bushberg JT, Boone JM. The Essential Physics of Medical Imaging. 3rd edition: Lippincott Williams and Wilkins; 2011.
26. Ren B, Ruth C, Wu T, Zhang Y, Smith A, Niklason L, *et al*. A new generation FFDM/tomosynthesis fusion system with selenium detector. SPIE Med Imaging 2010;7622:76220B.
27. Hernandez AM, Boone JM. Tungsten anode spectral model using interpolating cubic splines: Unfiltered x-ray spectra from 20 kV to 640 kV. Med Phys 2014;41:042101.
28. Okunade AA. Parameters and computer software for the evaluation of mass attenuation and mass energy-absorption coefficients for body tissues and substitutes. J Med Phys 2007;32:124-32.
29. Feng SS, Sechopoulos I. Clinical digital breast tomosynthesis system: Dosimetric characterization. Radiology 2012;263:35-42.